Networks and Heterogeneous Media

https://www.aimspress.com/journal/nhm

NHM, 21(1): 55–69.
DOI: 10.3934/nhm.2026003
Received: 19 August 2025
Revised: 19 December 2025
Accepted: 30 December 2025
Published: 16 January 2026

Research article

Exploring fractional dynamics in the fractional-in-time Gierer-Meinhardt reaction-diffusion model with periodic boundary condition

Xinzhi Wang[1] **and Wei Zhang**[2,*]

[1] School of Physics and Electronic Information Engineering, Jining Normal University, Ulanqab, Inner Mongolia 012000, China

[2] Institute of Economics and Management, Jining Normal University, Ulanqab, Inner Mongolia 012000, China

* **Correspondence:** Email: jnsfxyzw@163.com.

Abstract: This paper presents a new numerical method for simulating the dynamic behavior of the fractional-in-time Gierer-Meinhardt reaction-diffusion model with periodic boundary conditions. A recursive algorithm for binomial coefficients is introduced, avoiding numerical instabilities associated with Gamma functions. High-precision polynomial expansions and the short-memory principle are employed to enhance efficiency and accuracy. Numerical simulations reveal diverse pattern formation.

Keywords: fractional-in-time Gierer-Meinhardt model; pattern formation; numerical method; short-memory principle

1. Introduction

Fractional calculus, as a generalization of classical integer-order calculus, has gained considerable attention in recent decades due to its ability to model memory-dependent and non-local phenomena in various scientific and engineering fields. Foundational works by Oldham and Spanier [1], Miller and Ross [2], Podlubny [3], and Petráš [4] have laid the theoretical groundwork for fractional derivatives and integrals.

In recent years, the development of high-precision numerical methods for fractional differential equations has become a focal point in computational mathematics, driven by the need to accurately simulate systems with memory effects and non-local interactions. Various numerical approaches have been proposed, including finite difference, spectral methods, and optimization-based algorithms. For instance, Diethelm [5], and Li [6, 7] developed stable and efficient numerical schemes for fractional-order systems. Almatrafi developed efficient numerical schemes for solving fractional nonlinear wave equations, demonstrating superior accuracy and stability in long-time simulations [8, 9]. Wang et al. introduced a high-precision

Grünwald–Letnikov-based method for fractional dynamical systems such as the Hastings–Powell model, and conducted comprehensive numerical stability and convergence analyses [10]. In the context of financial systems, Gao et al. extended integer-order models to fractional settings and proposed a high-order numerical scheme to capture chaotic dynamics more effectively [11]. Che et al. applied Fourier spectral methods coupled with Runge–Kutta time integration to solve fractional reaction-diffusion models such as Gray–Scott and FitzHugh–Nagumo systems [12–14]. Zhu et al. combined network Laplacian operators with reaction-diffusion frameworks to model virus spread and green behavior propagation, employing multi-scale analysis and amplitude equations to predict pattern selection [15, 16]. Yang et al. incorporated optimal control theory into parameter identification for infectious disease models on complex networks [17]. Zhang et al. proposed a four-variable reaction-diffusion model and used a high-precision Fourier spectral method to simulate novel pattern morphologies [18]. Sha and Zhu further extended these methods to rumor propagation models, comparing different optimization algorithms for parameter convergence on various network topologies [19]. Shi and Zhu developed a theoretical and numerical framework for Turing patterns on higher-order temporal networks, revealing how oscillatory interactions influence pattern diversity [20]. Gao et al. numerically investigated a fractional vegetation-water model in arid environments, identifying fractal patterns and analyzing the impact of fractional order on pattern stability [21]. Li and Zhu analyzed Turing instability in rumor propagation systems with time delays, using linear stability analysis and numerical simulations to validate theoretical conditions [22]. Wang et al. also derived amplitude equations for a fractional Oregonator model and conducted extensive two-dimensional numerical experiments to confirm pattern predictions [23], and so on [24–26].

The classical Gierer-Meinhardt model (GMM) represented an activator-inhibitor system where one substance (the activator) promoted its own production along with the production of an inhibitor, which subsequently suppressed the activator.

The main numerical simulation methods for the Gierer-Meinhardt model include the finite difference method, the finite element method, the meshless method, and the spectral method. In [27], researchers employed a spectral collocation method to analyze the GMM, providing comparative analysis of when spectral methods were preferable to moving mesh methods. Their study encompassed both one- and two-dimensional systems, with results validated against a moving finite element method. Subsequent work [28] examined dynamical behaviors in an activator-inhibitor model with varied sources, where linear stability analysis yielded conditions for Turing bifurcation and derived amplitude equations. This research demonstrated various pattern formations supported by numerical simulations.The biological pattern formation aspects of GMM received particular attention in [29], where investigators focused on long-term solution behavior. They established that under specific conditions, solutions existed globally in time and eventually converged to periodic-in-time solutions, causing spatial patterns to disappear. Mathematical challenges in singular GMM with zero Dirichlet boundary conditions were addressed in [30] through innovative application of functional methods and Sobolev embedding theorems to prove existence of positive solutions. Further pattern generation mechanisms were explored in [31] for a generalized GMM with diffusion, where researchers established existence and stability conditions for Hopf bifurcation and derived Turing instability criteria, revealing both stripe and spot patterns through numerical simulations. The modified GMM with saturation term was investigated in [32], identifying parameter regions for Turing instability and deriving predictive amplitude equations, complemented by Fourier transform analysis of emerging patterns. Network effects on pattern formation were examined in [33], which analyzed

how system parameters, network topology, and average degree influenced Turing patterns in GMM on complex networks, proposing an exponential decay model for pattern prediction. Boundary condition effects were systematically studied in [34] through analysis of homogeneous Neumann conditions, combining eigenvalue analysis with numerical validation of stability and bifurcation results. Numerical approaches received particular attention, in [35], where an efficient moving mesh finite element method was employed to investigate spike pattern dynamics and instabilities. Existence proofs for generalized GMM solutions, particularly addressing singular nonlinearities near boundaries, were established in [36]. Time-delayed systems were analyzed in [37], deriving comprehensive conditions for various bifurcations and validating results through normal form analysis and numerical simulations.

Motivated by these advancements in numerical methods for fractional reaction-diffusion systems, in this paper, we propose a new high-precision numerical scheme for solving the time-fractional generalized Michaelis–Menten (GMM) system:

$$\begin{cases} \mathcal{D}_t^\alpha u = d_1 \nabla^2 u + \rho \dfrac{u^2}{v} - au + b, \\ \mathcal{D}_t^\alpha v = d_2 \nabla^2 v + \gamma(cu^2 - v), \end{cases} \tag{1.1}$$

where $a, b, c, \gamma, \rho, d_1$, and d_2 are all positive real numbers. $\mathcal{D}_t^\alpha u$, and $\mathcal{D}_t^\alpha v$ denote the Grünwald-Letnikov fractional derivative.

This paper makes the following main contributions:

- The first high-precision numerical scheme for the fractional-in-time Gierer–Meinhardt model with periodic boundaries.
- A new recursive binomial algorithm avoiding Gamma-function overflow, combined with a high-order polynomial expansion.
- Integration of the short-memory principle for efficient long-time pattern simulations, enabling the discovery of novel fractional-order-dependent patterns.

This paper is organized as follows. Section 2 introduces the numerical method and its implementation. Section 3 provides simulation results and pattern discussion. Finally, Section 4 concludes the paper.

2. Description of numerical method

Definition 2.1. *The α-th Grünwald-Letnikov fractional derivative for a function $f(t)$ is given by*

$$\mathcal{D}_t^\alpha f(t) = \lim_{h \to 0} \frac{1}{\tau^\alpha} \sum_{j=0}^{\left\lfloor \frac{t-t_0}{\tau} \right\rfloor} (-1)^j \binom{\alpha}{j} f(t - jh), t \in [t_0, t]. \tag{2.1}$$

where $[\cdot]$ denotes the nearest integer function. $(-1)^j\binom{\alpha}{j}$ is the binomial coefficient, and

$$c_j = (-1)^j \binom{\alpha}{j} = (-1)^j \frac{\Gamma(\alpha + 1)}{\Gamma(j + 1)\Gamma(\alpha - j + 1)}. \tag{2.2}$$

The numerical calculation of the α-th Grünwald–Letnikov fractional derivative can be directly computed by the following formula:

$$\mathcal{D}_t^\alpha f(t) \approx \frac{1}{\tau^\alpha} \sum_{j=0}^{\left\lfloor \frac{t-t_0}{\tau} \right\rfloor} c_j f(t - jh). \tag{2.3}$$

For the numerical computation of the α-th Grünwald–Letnikov fractional derivative in Eq (2.3), direct implementation of the definition involves calculating Gamma function values for large numbers. However, terms including $\Gamma(172)$ and subsequent values become infinite (Inf) under MATLAB's double-precision arithmetic. This leads to unavoidable computational errors when using the Gamma function to compute binomial coefficients. To address this issue, a more reliable approach for computing GL fractional derivatives is required. Specifically, we employ the following recursive algorithm to calculate binomial coefficients while avoiding the use of Gamma functions.

$$c_0 = 1, \quad c_j = \left(1 - \frac{\alpha + 1}{j}\right) c_{j-1}, \quad j = 1, 2, \cdots \tag{2.4}$$

Thus, by recursively computing the binomial coefficients w_j using Eq (2.4), we can directly evaluate the fractional derivative of a given function via Eq (2.3). Since the recursive algorithm successfully avoids explicit computation of Gamma functions, it resolves the numerical issues inherent in the direct implementation of the definition. Moreover, it can be shown that this algorithm achieves an accuracy of $o(h)$.

To improve computational precision, one may replace the binomial expansion in the recursive formula for the Grünwald-Letnikov fractional derivative with a polynomial expansion. We explore the construction methods for such generating functions.

Definition 2.2. *A p-order polynomial generating function of first-order derivative is defined as:*

$$g_p(z) = \sum_{k=1}^{p} \frac{1}{k}(1 - z)^k. \tag{2.5}$$

Here, p is a positive integer.

For p-order generating functions, the following theorem holds:

Theorem 2.3. *The p-order generating function $g_p(z)$ can be expressed as a polynomial:*

$$g_p(z) = \sum_{k=0}^{p} a_k z^k, \tag{2.6}$$

where the coefficients g_k can be computed directly from the following matrix equation:

$$\begin{cases} a_0 + a_1 + a_2 + \cdots + a_p = 0, \\ a_0 + 2a_1 + 3a_2 + \cdots + (p+1)a_p = -1, \\ a_0 + 2^2 a_1 + 3^2 a_2 + \cdots + (p+1)^2 a_p = -2, \\ \vdots \\ a_0 + 2^p a_1 + 3^p a_2 + \cdots + (p+1)^p a_p = -p. \end{cases} \tag{2.7}$$

Proof. From formulas (2.5) and (2.6), we have

$$\sum_{k=0}^{p} a_k z^k = \sum_{k=1}^{p} \frac{1}{k}(1 - z)^k. \tag{2.8}$$

Substituting $z = 1$ into formula (2.8), we have

$$\sum_{k=0}^{p} a_k = 0. \tag{2.9}$$

Multiplying both sides of formula (2.8) by z and then taking the first derivative with respect to z, we have

$$\sum_{k=0}^{p}(k+1)a_k z^k = \sum_{k=1}^{p}\frac{1}{k}(1-z)^k - z\sum_{k=1}^{p}(1-z)^{k-1}. \tag{2.10}$$

Substituting $z = 1$ into formula (2.10), we have

$$\sum_{k=0}^{p}(k+1)a_k = -1.$$

Multiplying both sides of formula (2.10) by z and taking the first derivative with respect to z again , we have

$$\sum_{k=0}^{p}(k+1)^2 a_k z^k = \sum_{k=1}^{p}\frac{1}{k}(1-z)^k - 3z\sum_{k=1}^{p}(1-z)^{k-1} + z^2\sum_{k=2}^{p}\frac{1}{k-1}(1-z)^{k-2}. \tag{2.11}$$

Substituting $z = 1$ into formula (2.11) leads to

$$\sum_{k=0}^{p}(k+1)^2 a_k = -2.$$

Repeating this process, we can establish the Eq (2.7).

Definition 2.4. *The p-order generating function with fractional derivative α is defined as:*

$$g_p^{\alpha}(z) = (a_0 + a_1 z + \cdots + a_p z^p)^{\alpha}.$$

Theorem 2.5. *Taylor series expansion of the p-order generating function $g_p^{\alpha}(z)$ with the fractional derivative α can be written as*

$$g_p^{\alpha}(z) = \sum_{k=0}^{\infty} c_k^{\alpha} z^k,$$

where,

$$\begin{aligned} c_0 &= g_0, \\ c_m &= -\frac{1}{g_0}\sum_{i=1}^{m-1} g_i\left(1 - i\frac{1+\alpha}{m}\right)c_{m-i}, \quad \text{for } m = 1, 2, \cdots, p-1, \\ c_k &= -\frac{1}{g_0}\sum_{i=1}^{p} g_i\left(1 - i\frac{1+\alpha}{k}\right)c_{k-i}, \quad \text{for } k = p, p+1, p+2, \cdots. \end{aligned} \tag{2.12}$$

If the binomial coefficients here are replaced by high-precision polynomials of order $o(h^p)$, we can define a high-precision algorithm. The high-precision numerical calculation of the Grünwald–Letnikov fractional derivative can be directly computed by the following formula:

$${}_{t_0}\mathcal{D}_t^{\alpha} f(t) \approx \frac{1}{\tau^{\alpha}}\sum_{j=0}^{\left\lfloor\frac{t-t_0}{\tau}\right\rfloor} c_j f(t - jh). \tag{2.13}$$

where c_j is shown in formula (2.12).

Next, we present the numerical method for solving the fractional partial differential Eq (1.1).

The uniform spatial grid is:

$$\begin{aligned} x_i &= ih, \quad i = 0, \ldots, N-1, \\ y_j &= jh, \quad j = 0, \ldots, N-1, \\ t_k &= k\tau t, \quad k = 0, \ldots, M. \end{aligned}$$

where $u(x_i, y_j, t_k) \approx u_{i,j}^k$, $v(x_i, y_j, t_k) \approx v_{i,j}^k$.

The initial conditions are discretized as:

$$u_{i,j}^0 = v_{i,j}^0 = \begin{cases} 0.5 + 0.1\xi_{i,j} & \text{for } 80 \le i, j \le N - 80. \\ 0.1\xi_{i,j} & \text{otherwise,} \end{cases} \qquad \xi_{i,j} \sim \mathcal{U}[-0.5, 0.5].$$

The periodic boundary conditions are implemented as:

$$\begin{aligned} &u_{0,j} = u_{N,j}, && u_{N+1,j} = u_{1,j}, && u_{i,0} = u_{i,N}, && u_{i,N+1} = u_{i,1}, \\ &v_{0,j} = v_{N,j}, && v_{N+1,j} = v_{1,j}, && v_{i,0} = v_{i,N}, && v_{i,N+1} = v_{i,1}, \end{aligned}$$

with special handling for the corners.

$$\begin{aligned} &u_{0,0} = u_{N,N}, && u_{0,N} = u_{N,0}, && u_{N,0} = u_{0,N}, && u_{N,N} = u_{0,0}, \\ &v_{0,0} = v_{N,N}, && v_{0,N} = v_{N,0}, && v_{N,0} = v_{0,N}, && v_{N,N} = v_{0,0}. \end{aligned}$$

For boundary points, the Laplacian is computed with periodic conditions.

$$\begin{aligned} \Delta_h u_{1,j}^k &= u_{2,j}^k + u_{N,j}^k + u_{1,j+1}^k + u_{1,j-1}^k - 4u_{1,j}^k, & \Delta_h u_{N,j}^k &= u_{1,j}^k + u_{N-1,j}^k + u_{N,j+1}^k + u_{N,j-1}^k - 4u_{N,j}^k, \\ \Delta_h u_{i,1}^k &= u_{i+1,1}^k + u_{i-1,1}^k + u_{i,2}^k + u_{i,N}^k - 4u_{i,1}^k, & \Delta_h u_{i,N}^k &= u_{i+1,N}^k + u_{i-1,N}^k + u_{i,1}^k + u_{i,N-1}^k - 4u_{i,N}^k, \end{aligned}$$

and similarly for v.

At the interior points $(i, j) \in [2, N-1] \times [2, N-1]$, the calculation formula is

$$\begin{aligned} \Delta_h u_{i,j}^k &= u_{i+1,j}^k + u_{i-1,j}^k + u_{i,j+1}^k + u_{i,j-1}^k - 4u_{i,j}^k, \\ \Delta_h v_{i,j}^k &= v_{i+1,j}^k + v_{i-1,j}^k + v_{i,j+1}^k + v_{i,j-1}^k - 4v_{i,j}^k. \end{aligned}$$

Using Eq 2.13, a high-precision computational format of Eq 1.1 is given by

$$\begin{cases} \dfrac{u_{i,j}^{k+1} - \sum_{m=0}^{k} c_m u_{i,j}^{k-m}}{\tau^\alpha} = d_1 \Delta_h u_{i,j}^k + \mathrm{NL}_1(u_{i,j}^k, v_{i,j}^k), \\ \dfrac{v_{i,j}^{k+1} - \sum_{m=0}^{k} c_m v_{i,j}^{k-m}}{\tau^\alpha} = d_2 \Delta_h v_{i,j}^k + \mathrm{NL}_2(v_{i,j}^k, u_{i,j}^k), \end{cases} \tag{2.14}$$

where $\mathrm{NL}_1(u, v) = \rho \dfrac{u^2}{v} - au + b, \mathrm{NL}_2(u, v) = \gamma(cu^2 - v)$.

In general cases, if the computation step size h is chosen too small or the value $[t/h]$ becomes too large, the number of points involved in the summation in Eq (2.13) can become extremely large,

potentially leading to significantly increased computational load. When the computation becomes infeasible, we should consider reducing the number of computation points. In practical applications, computing fractional derivatives does not necessarily require using all historical information from $[t/h]$; using only recent information from the time interval $[t - L, t]$ can reduce the computational load [28]:

$$ {}_{t_0}\mathcal{D}_t^{\alpha} f(t) \approx_{t-L} \mathcal{D}_t^{\alpha} f(t). $$

This method is called the short-memory effect [3, 38]. Using this approach, the Grünwald–Letnikov fractional derivative can be approximated as:

$$ y(t) \approx \frac{1}{h^{\alpha}} \sum_{j=0}^{N(t)} c_j f(t - jh), $$

where $N(t) = \min\left\{\left\lfloor \frac{t}{\tau} \right\rfloor, \frac{L}{h}\right\}$. L is called the memory length. To improve computational efficiency for large-scale simulations, we can leverage the short-memory principle: Using Eq (2.13), a high precision computational format with the short-memory principle of Eq (1.1) is:

$$ \begin{cases} u_{i,j}^{k+1} = \tau^{\alpha}\left(d_1 \Delta_h u_{i,j}^{k} + \mathrm{NL}_1(u_{i,j}^{k}, v_{i,j}^{k})\right) + \mathrm{Memo}(u, c, k), \\ v_{i,j}^{k+1} = \tau^{\alpha}\left(d_2 \Delta_h v_{i,j}^{k} + \mathrm{NL}_2(v_{i,j}^{k}, u_{i,j}^{k})\right) + \mathrm{Memo}(v, c, k), \end{cases} \tag{2.15} $$

where $\mathrm{NL}_1(u, v) = \rho\dfrac{u^2}{v} - au + b$, and $\mathrm{NL}_2(u, v) = \gamma(cu^2 - v)$. c_k is shown in Eq (2.12). The memory term is $\mathrm{Memo}(u, c, k) = \sum_{m=0}^{N(t)} c_m u_{i,j}^{k-m}$, and similarly for v.

3. Numerical simulation

The solution obtained by ode45 is taken as the fundamental solution. The effectiveness of the present method can be seen from Figure 1. Using the present method, we discover some novel dynamic behaviors, which are shown in Figures 1–6. For $\alpha = 1$, the time derivative can be calculated using the Euler format. The method can be extended and applied to 3D space. 3D patterns are shown in Figure 5.

Figure 1 compares the absolute errors of different numerical methods (the GL method, closed-form solution, the proposed method, and predictor-corrector methods) under specific parameters: $d_1 = 0, d_2 = 0, \rho = 0.5, a = 0.15, b = 0.1, \gamma = 0.2, c = 0.3, \tau = 0.0001$, and $\alpha = 1$. This figure validates the accuracy and superiority of the proposed high-precision numerical scheme in the integer-order case ($\alpha = 1$).

Figure 2 compares dynamic behaviors under different fractional derivative orders (α, α) with initial condition $x_0 = [3, 5]$ and parameters $\tau = 0.1, t = 300, d_1 = d_2 = 0, \gamma = 0.3$, and $c = 0.8$. This figure reveals the significant influence of the fractional derivative order on the system's dynamics, indicating that α is a key parameter controlling pattern selection.

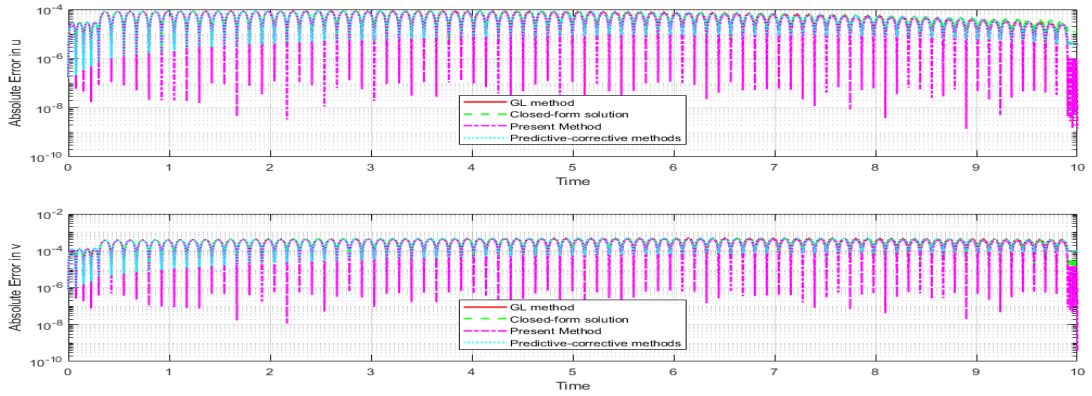

Figure 1. Comparing the absolute error for the GL method, closed-form solution, present method, and the predictive-corrective methods at $d_1 = 0, d_2 = 0, rho = 0.5, a = 0.15, b = 0.1, \gamma = 0.2, c = 0.3, \tau = 0.0001, \alpha = 1$.

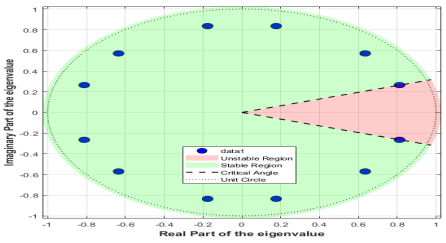

Stability at $\rho = 1.0, a = 0.5, b = 1.0, \alpha = 1.2$

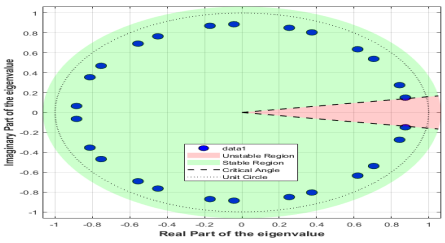

Stability at $\rho = 0.8, a = 0.15, b = 0.4, \alpha = 1.3$

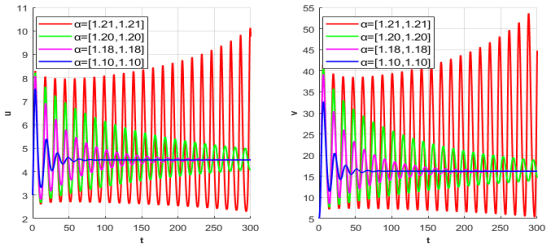

Time series at $\rho = 1.0, a = 0.5, b = 1.0$

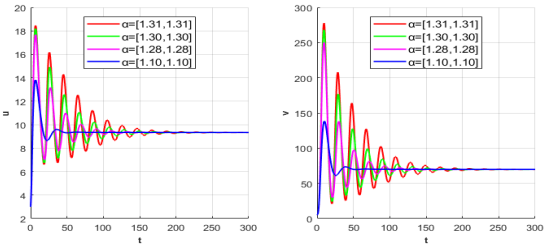

Time series at $\rho = 0.8, a = 0.15, b = 0.4$

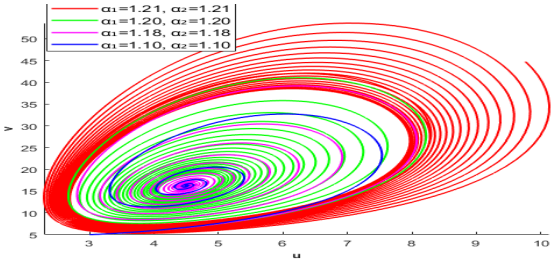

Phase diagram at $\rho = 1.0, a = 0.5, b = 1.0$

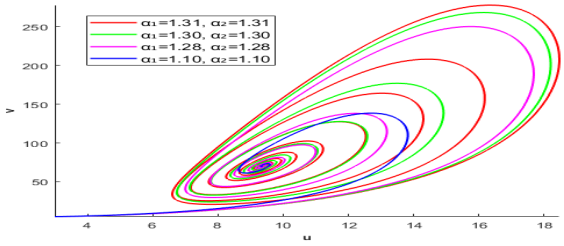

Phase diagram at $\rho = 0.8, a = 0.15, b = 0.4$

Figure 2. Comparison of dynamic behavior at different fractional derivative $(\alpha, \alpha), x_0 = [3, 5], \tau = 0.1, t = 300, d_1 = d_2 = 0, \gamma = 0.3$, and $c = 0.8$.

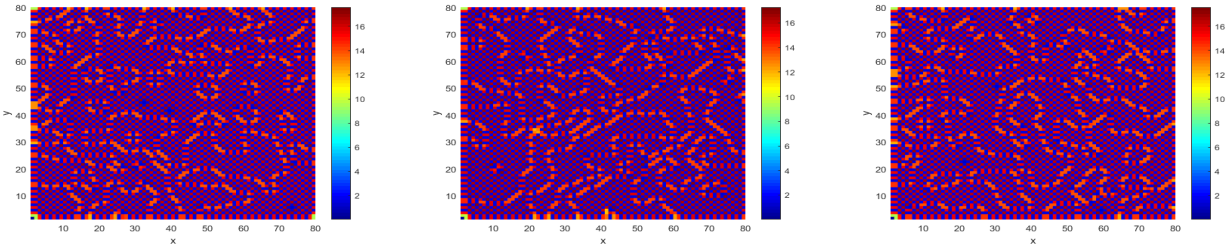

u at $\alpha = 0.998$ u at $\alpha = 0.999$ u at $\alpha = 1$

Figure 3. Pattern dynamic behavior at $d_1 = 0.0011, d_2 = 0.029, \tau = 0.09, h = 0.8, M = 40,000, M = 80, \rho = 0.5, a = 0.15, b = 0.1, \gamma = 0.2$, and $c = 0.3$.

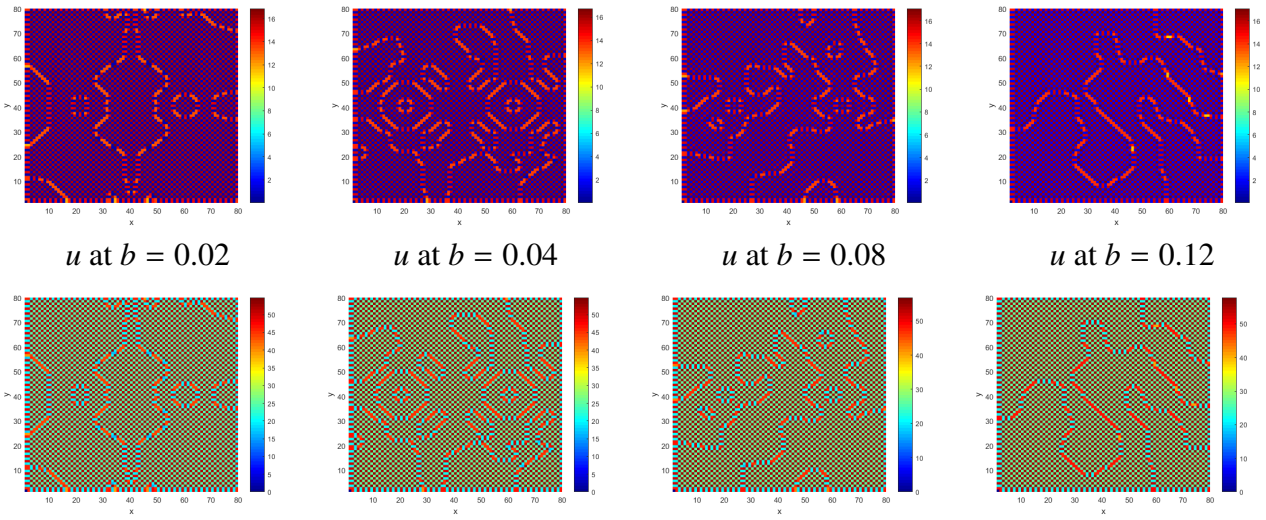

u at $b = 0.02$ u at $b = 0.04$ u at $b = 0.08$ u at $b = 0.12$

v at $b = 0.02$ v at $b = 0.04$ v at $b = 0.08$ v at $b = 0.12$

Figure 4. Pattern dynamic behavior at $d_1 = 0.0011, d_2 = 0.029, \tau = 0.09, h = 0.8, M = 80,000, N = 80, \rho = 0.5, a = 0.15, \gamma = 0.2$, and $c = 0.3, \alpha = 1$.

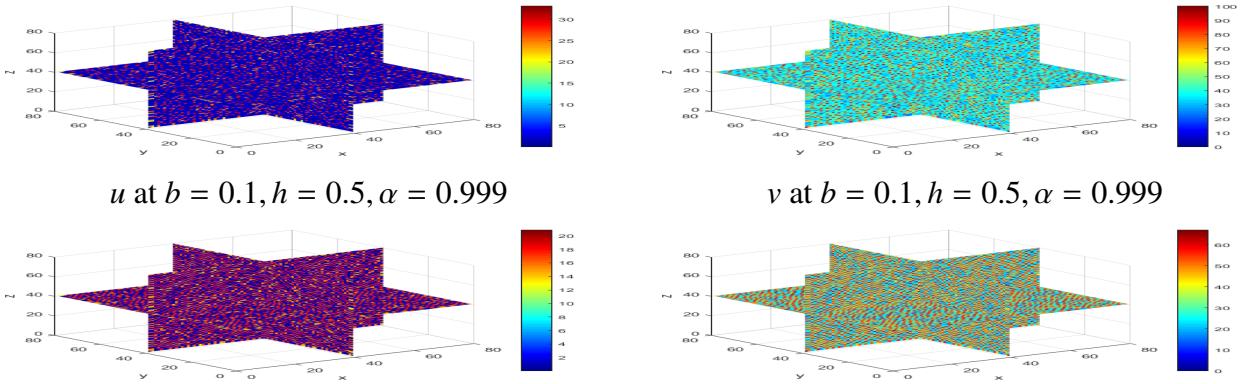

u at $b = 0.1, h = 0.5, \alpha = 0.999$ v at $b = 0.1, h = 0.5, \alpha = 0.999$

u at $b = 0.04, h = 0.8, \alpha = 0.998$ v at $b = 0.04, h = 0.8, \alpha = 0.998$

Figure 5. Pattern dynamic behavior at $d_1 = 0.0011, d_2 = 0.029, \alpha = 2.5, \tau = 0.09, M = 80,000, N = 80, \rho = 0.5, a = 0.15, \gamma = 0.2$, and $c = 0.3$.

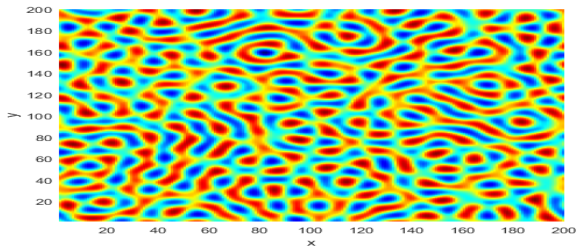

u at $d_1 = 0.2, d_2 = 2.3, \alpha = 1$

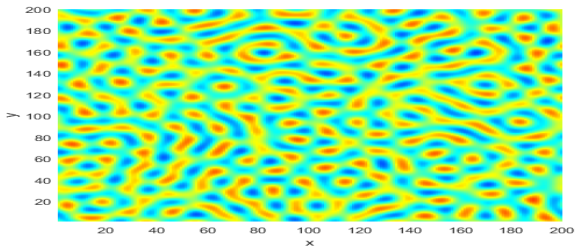

v at $d_1 = 0.2, d_2 = 2.3, \alpha = 1$

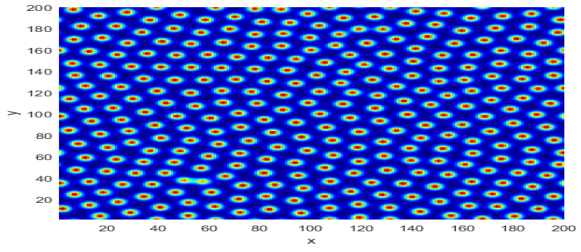

u at $d_1 = 0.1, d_2 = 2.5, \alpha = 1$

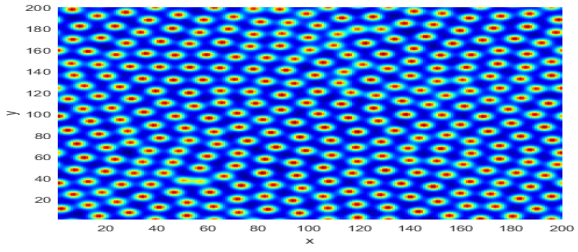

v at $d_1 = 0.1, d_2 = 2.5, \alpha = 1$

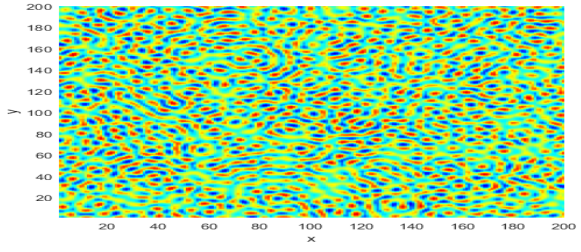

u at $d_1 = 0.05, d_2 = 0.5, \alpha = 0.999$

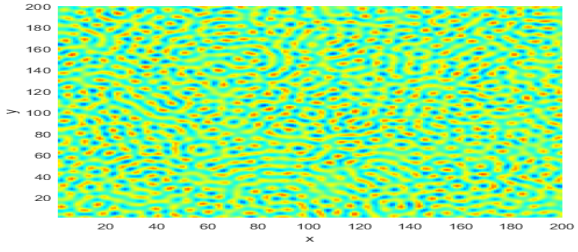

v at $d_1 = 0.05, d_2 = 0.5, \alpha = 0.999$

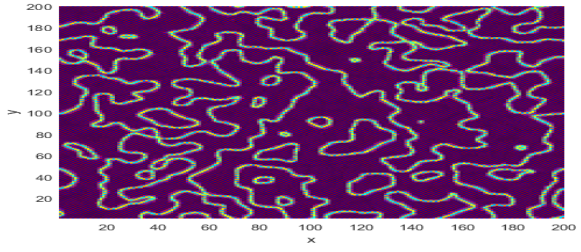

u at $d_1 = 0.0011, d_2 = 0.029, \alpha = 1$

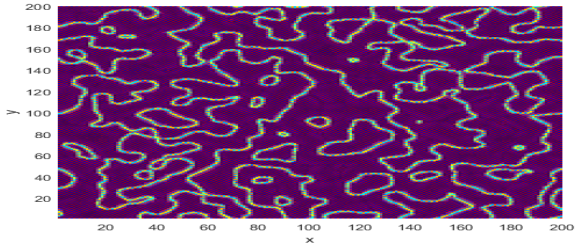

v at $d_1 = 0.0011, d_2 = 0.029, \alpha = 1$

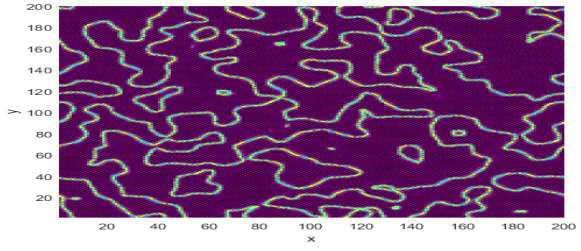

u at $d_1 = 0.0011, d_2 = 0.029, \alpha = 1.001$

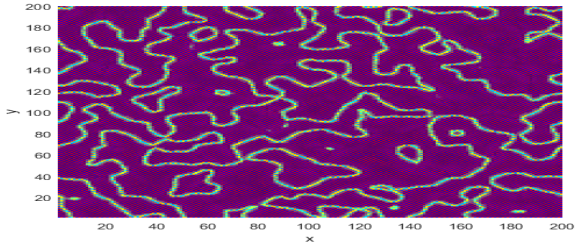

v at $d_1 = 0.0011, d_2 = 0.029, \alpha = 1.001$

Figure 6. Pattern dynamic behavior at $d_1 = 0.2, d_2 = 2.3, \tau = 0.1, h = 1, M = 20,000, N = 200, \rho = 1.0, a = 0.1, b = 0.5, \gamma = 0.2$, and $c = 0.3$.

Figure 3 shows pattern dynamic behavior for $\alpha = 0.998, 0.999$, and 1 at the parameters $d_1 = 0.0011, d_2 = 0.029, \tau = 0.09, h = 0.8, M = 40,000, N = 80, \rho = 0.5, a = 0.15, b = 0.1, \gamma = 0.2$, and $c = 0.3$. The figure displays spatial distributions of the u component for different α values, showing that as α approaches 1, the pattern structure gradually becomes more stable and regular.

Figure 4 Explores pattern dynamic behavior for different values of b (0.02, 0.04, 0.08, 0.12) with other parameters $d_1 = 0.0011, d_2 = 0.029, \tau = 0.09, h = 0.8, M = 80,000, N = 80, \rho = 0.5, a = 0.15, \gamma = 0.2, c = 0.3$, and $\alpha = 1$. The figure presents pattern evolution of both u and v components as b varies, indicating that the parameter b modulates pattern morphology.

Figure 5 displays pattern dynamic behavior for different combinations of b and h with $\alpha = 0.999$ and $\alpha = 0.998$, at parameters $d_1 = 0.0011, d_2 = 0.029, \tau = 0.09, M = 80,000, N = 80, \rho = 0.5, a = 0.15, \gamma = 0.2$, and $c = 0.3$. This figure further validates the coupled influence of fractional derivative order and spatial step size on pattern formation.

Figure 6 shows the pattern structure of the v component under parameters $d_1 = 0.2, d_2 = 2.3$, and $\alpha = 1$, illustrating pattern characteristics when diffusion coefficients are relatively large, potentially related to spot or stripe Turing patterns.

4. Discussion and conclusions

This paper presents a high-precision numerical method for the fractional Gierer-Meinhardt model, successfully applied to systems with periodic boundary conditions. By introducing a recursive algorithm for binomial coefficients and employing high-order polynomial expansions, the method effectively avoids numerical instabilities associated with Gamma functions. Combined with the short-memory principle, the approach significantly improves computational efficiency for long-time simulations while maintaining accuracy.

Numerical simulation results (Figures 1–6) systematically demonstrate the regulatory effects of the fractional derivative α, system parameters (such as b, d_1, d_2), and spatial step size h on pattern formation. In particular, Figures 2 and 3 show that as α approaches 1, the system's dynamic behavior gradually converges to that of the classical integer-order model, while still retaining the memory and non-local effects characteristic of fractional-order systems. Figure 4 further reveals the role of the parameter b in balancing the activator-inhibitor dynamics, where its variation can induce various Turing patterns, from spot-like to stripe-like structures.

It is noteworthy that the proposed method demonstrates comparable accuracy to traditional methods in the integer-order case (Figure 1), while stably capturing complex spatiotemporal patterns in fractional-order cases (Figures 3 and 5). These results validate the robustness and applicability of the proposed numerical framework.

However, although the short-memory principle significantly enhances computational efficiency, its theoretical error bounds in strongly memory-dependent systems require further investigation. Future work could explore adaptive memory length selection strategies, extensions to non-uniform boundary conditions, and the method's potential applications in three-dimensional or higher-dimensional systems.

In summary, this study provides a reliable and efficient tool for the numerical simulation of fractional reaction-diffusion systems. It reveals the profound influence of the fractional derivative on pattern selection mechanisms within the Gierer-Meinhardt model, offering new computational insights for understanding complex processes such as biological morphogenesis and ecological pattern formation.

Use of AI tools declaration

The authors declare we have not used Artificial Intelligence (AI) tools in the creation of this article.

Acknowledgements

This paper is supported by Inner Mongolia Jining Teachers College Natural Science Key Research Project (JSKY2024006).

Conflicts of interest

The authors declare that there are no conflicts of interest regarding the publication of this article.

Author contributions

Conceptualization, Methodology, Software, Data, Formal analysis and Funding acquisition, Writing-original draft and writing review and editing: Xin Zhi Wang and Wei Zhang. All authors have read and agreed to the published version of the manuscript.

Data availability

The data used to support the findings of this study are available from the corresponding author upon request.

References

1. K. B. Oldham, J. Spanier, *The Fractional Calculus: Theory and Applications of Differentiation and Integration to Arbitrary Order*, Academic Press: New York, NY, USA, 1974. https://doi.org/10.1016/s0076-5392(09)x6012-1
2. K. S. Miller, B. Ross, *An Introduction to the Fractional Calculus and Fractional Differential Equations*, John Wiley & Sons: New York, NY, USA, 1993.
3. I. Podlubny, *Fractional Differential Equations*, Academic Press: San Diego, CA, USA, 1999. https://doi.org/10.1016/s0076-5392(99)x8001-5
4. I. Petráš, *Fractional-Order Nonlinear Systems, Modeling, Analysis and Simulation*, Springer: Heidelberg, Germany, 2011. https://doi.org/10.1007/978-3-642-18101-6
5. K. Diethelm, *The Analysis of Fractional Differential Equations: An Application-Oriented Exposition Using Differential Operators of Caputo Type*, Springer-Verlag, 2010. https://doi.org/10.1007/978-3-642-14574-2
6. C. P. Li, F. H. Zeng, *Numerical Methods for Fractional Calculus*, CRC Press, Boca Raton, 2015. https://doi.org/10.1201/b18503

7. C. P. Li, M. Cai, *Theory and Numerical Approximations of Fractional Integrals and Derivatives*, Society for Industrial and Applied Mathematics, Philadelphia, 2020. https://doi.org/10.1137/1.9781611975888

8. M. B. Almatrafi, Abundant traveling wave and numerical solutions for Novikov-Veselov system with their stability and accuracy, *Appl. Anal.*, **102** (2023), 2389–2402. https://doi.org/10.1080/00036811.2022.2027381

9. H. L. Zhang, Z. Y. Li, X. Y Li. Numerical simulation of pattern and chaos dynamic behaviour in the fractional-order-in-time Lengyel-Epstein reaction-diffusion system, *Int. J. Comput. Math.*, https://doi.org/10.1080/00207160.2025.2612196

10. X. H. Wang, H. L. Zhang, Y. L. Wang, Z. Y. Li, Dynamic properties and numerical simulations of the fractional Hastings–Powell model with the Grünwald–Letnikov differential derivative, *Int. J. Bifurcat. Chaos*, **35** (2025), 1250145. https://doi.org/10.1142/S0218127425501457

11. X. L. Gao, Z. Y. Li, Y. L. Wang, Chaotic dynamic behavior of a fractional-order financial system with constant inelastic demand, *Int. J. Bifurcat. Chaos*, **34** (2024), 2450111. https://doi.org/10.1142/S0218127424501116

12. H. Che, Y. L. Wang, Z. Y. Li, Novel patterns in a class of fractional reaction-diffusion models with the Riesz fractional derivative, *Math. Comput. Simul.*, **202** (2022), 149–163. https://doi.org/10.1016/j.matcom.2022.05.037

13. C. Han, Y. L. Wang, Z. Y. Li, A high-precision numerical approach to solving space fractional Gray-Scott model, *Appl. Math. Lett.*, **125** (2022), 107759. https://doi.org/10.1016/j.aml.2021.107759

14. C. Han, Y. L. Wang, Z. Y. Li, Numerical solutions of space fractional variable-coefficient KdV-modified KdV equation by Fourier spectral method, *Fractals*, **29** (2021), 2150246. https://doi.org/10.1142/S0218348X21502467

15. L. Zhu, T. Zheng, Pattern dynamics analysis and application of West Nile virus spatiotemporal models based on higher-order network topology, *Bull. Math. Biol.*, **87** (2025), 121. https://doi.org/10.1007/s11538-025-01501-6

16. L. Zhu, Y. Ding, S. Shen, Green behavior propagation analysis based on statistical theory and intelligent algorithm in data-driven environment, *Math. Biosci.*, **379** (2025), 109340. https://doi.org/10.1016/j.mbs.2024.109340

17. T. Yang, L. Zhu, S. Shen, L. He, Pattern dynamics analysis and parameter identification of spatiotemporal infectious disease models on complex networks, *Math. Biosci.*, **387** (2025), 109502. https://doi.org/10.1016/j.mbs.2025.109502

18. H. L. Zhang, Y. L. Wang, J. X. Bi, S. H. Bao, Novel pattern dynamics in a vegetation-water reaction-diffusion model, *Math. Comput. Simul.*, **241** (2026), 97–116. https://doi.org/10.1016/j.matcom.2025.09.020

19. H. Sha, L. Zhu, Dynamic analysis of pattern and optimal control research of rumor propagation model on different networks, *Inf. Process. Manage.*, **62** (2025), 104016. https://doi.org/10.1016/j.ipm.2024.104016

20. J. Shi, L. Zhu, Turing pattern theory on homogeneous and heterogeneous higher-order temporal network system, *J. Math. Phys.*, **66** (2025), 042706. https://doi.org/10.1063/5.0211728

21. X. L. Gao, H. L. Zhang, Y. L. Wang, Z. Y. Li, Research on pattern dynamics behavior of a fractional vegetation-water model in arid flat environment, *Fractal Fract.*, **8** (2024), 264. https://doi.org/10.3390/fractalfract8050264

22. B. Li, L. Zhu, Turing instability analysis of a reaction–diffusion system for rumor propagation in continuous space and complex networks, *Inf. Process. Manage.*, **61** (2024), 103621. https://doi.org/10.1016/j.ipm.2023.103621

23. J. Y. Yang, Y. L. Wang, Z. Y. Li, Exploring dynamics and pattern formation of a fractional-order three-variable Oregonator model, *Netw. Heterog. Media*, **20** (2025), 1201–1229. https://doi.org/10.3934/nhm.2025052

24. J. Ning, Y. L. Wang, Fourier spectral method for solving fractional-in-space variable coefficient KdV-Burgers equation, *Indian J. Phys.*, **98** (2024), 1727–1744. https://doi.org/10.1007/s12648-023-02934-2

25. X. L. Gao, H. L. Zhang, X. Y. Li, Research on pattern dynamics of a class of predator-prey model with interval biological coefficients for capture, *AIMS Math.*, **9** (2024), 18506–18527. https://doi.org/10.3934/math.2024901

26. S. Zhang, H. L. Zhang, Y. L. Wang, Z. Y. Li, Dynamic properties and numerical simulations of a fractional phytoplankton-zooplankton ecological model, *Netw. Heterog. Media*, **20** (2025), 648–669. https://doi.org/10.3934/nhm.2025028

27. M. McCourt, N. Dovidio, M. Gilbert, Spectral methods for resolving spike dynamics in the Geirer-Meinhardt model, *Commun. Comput. Phys.*, **3** (2008), 659–678.

28. G. Q. Sun, C. H. Wang, Z. Y. Wu, Pattern dynamics of a Gierer-Meinhardt model with spatial effects, *Nonlinear Dyn.*, **88** (2017), 1385–1396. https://doi.org/10.1007/s11071-016-3317-9

29. G. Karali, T. Suzuki, Y. Yamada, Global-in-time behavior of the solution to a Gierer-Meinhardt system, *Discrete Contin. Dyn. Syst.*, **33** (2013), 2885–2900. https://doi.org/10.3934/dcds.2013.33.2885

30. S. Chen, Y. Salmaniw, R. Xu, Global existence for a singular Gierer-Meinhardt system, *J. Differ. Equations*, **262** (2017), 2940–2960. https://doi.org/10.1016/j.jde.2016.11.022

31. J. Wang, Y. Li, X. Hou, Supercritical Hopf bifurcation and Turing patterns for an activator and inhibitor model with different sources, *Adv. Differ. Equ.*, **2018** (2018), 241. https://doi.org/10.1186/s13662-018-1697-5

32. Y. Song, R. Yang, G. Sun, Pattern dynamics in a Gierer-Meinhardt model with a saturating term, *Appl. Math. Model.*, **46** (2017), 476–491. https://doi.org/10.1016/j.apm.2017.01.081

33. L. Guo, X. Shi, J. Cao, Turing patterns of Gierer-Meinhardt model on complex networks, *Nonlinear Dyn.*, **105** (2021), 899–909. https://doi.org/10.1007/s11071-021-06618-6

34. X. P. Yan, Y. J. Ding, C. H. Zhang, Dynamics analysis in a Gierer-Meinhardt reaction-diffusion model with homogeneous Neumann boundary condition, *Int. J. Bifurcat. Chaos*, **29** (2019), 1930025. https://doi.org/10.1142/S0218127419300258

35. Z. Qiao, Numerical investigations of the dynamical behaviors and instabilities for the Gierer-Meinhardt system, *Commun. Comput. Phys.*, **3** (2008), 406–426.

36. Y. S. Choi, P. J. McKenna, A singular Gierer-Meinhardt system of elliptic equations: The classical case, *Nonlinear Anal.*, **55** (2003), 521–541. https://doi.org/10.1016/j.na.2003.07.003

37. R. Yang, X. Q. Yu, Turing-Hopf bifurcation in diffusive Gierer-Meinhardt model, *Int. J. Bifurcat. Chaos*, **32** (2022), 2250046. https://doi.org/10.1142/S0218127422500468

38. D. Y. Xue, L. Bai, Numerical algorithms for Caputo fractional-order differential equations, *Int. J. Control*, **90** (2016), 1201–1211. https://doi.org/10.1080/00207179.2016.1158419

AIMS Press